Structural Engineering and Mechanics, Vol. 5, No. 2 (1997) 149-165
DOI: http://dx.doi.org/10.12989/sem.1997.5.2.149

Axial response of PWR fuel assemblies for earthquake and pipe break excitations

Myung J. Jhung†

Mechanical Engineering Group, Korea Institute of Nuclear Safety, Taejon, 305-338, Korea

Abstract. A dynamic time-history analysis of the coupled internals and core in the vertical direction is performed as a part of the fuel assembly qualification program. To reflect the interaction between the fuel rods and grid cage, friction element is developed and is implemented. Also derived here is a method to calculate a hydraulic force on the reactor internals due to pipe break. Peak responses are obtained for the excitations induced from earthquake and pipe break. The dynamic responses such as fuel assembly axial forces and lift-off characteristics are investigated.

Key words: reactor internals; fuel assembly; pressurized water reactor; pipe break; earthquake.

1. Introduction

The reactor core of a pressurized water reactor (PWR) is composed of several hundreds of assemblies of different kinds such as ordinary fuel assemblies and control element assemblies. They are rectangular beams supported by a fuel alignment plate (FAP) and a core support plate (CSP) at the top and bottom ends, respectively, immersed in coolant with very narrow spacings between adjacent assemblies. The guide tubes, the structural frame of the assembly, are individually fitted into circular tubes and pins held by the FAP and CSP, respectively (Fig. 1). They are positioned by preload only and are not restrained mechanically in the vertical direction. As a result, the fuel assemblies may suffer uplift when they are excited by a large vertical dynamic motion. Thus, in an earthquake or pipe break event, their vibratory motions may have a complicated nature including non-linearity due to the effects of frictions between fuel rods and grid cage.

Safety qualification of the reactor core is one of the crucial issues in the faulted condition design of a PWR, and it should be secured that the structural integrity of the fuel assemblies and the vertical height of the guide pins be not exceeded against the design loads. The procedure of analysis is described briefly as follows. As the first step, reactor vessel motion is obtained from the reactor coolant system analysis in which a very simplified model of the internals and core is used. Subsequently, the reactor vessel (RV) motion is used as an input to a coupled model of internals and core. The analysis of internals and core generates design loads of reactor internals and fuel assembly. Fig. 2 illustrates the overall design analysis flow. For the pipe break analysis, the hydraulic loads as well as reactor vessel motions are used as forcing terms. But there exists no hydraulic load for the earthquake excitation and also it is negligible for the secondary side pipe breaks. Therefore, activities 1 through 4 in Fig. 2 are not necessary for

† Senior Researcher

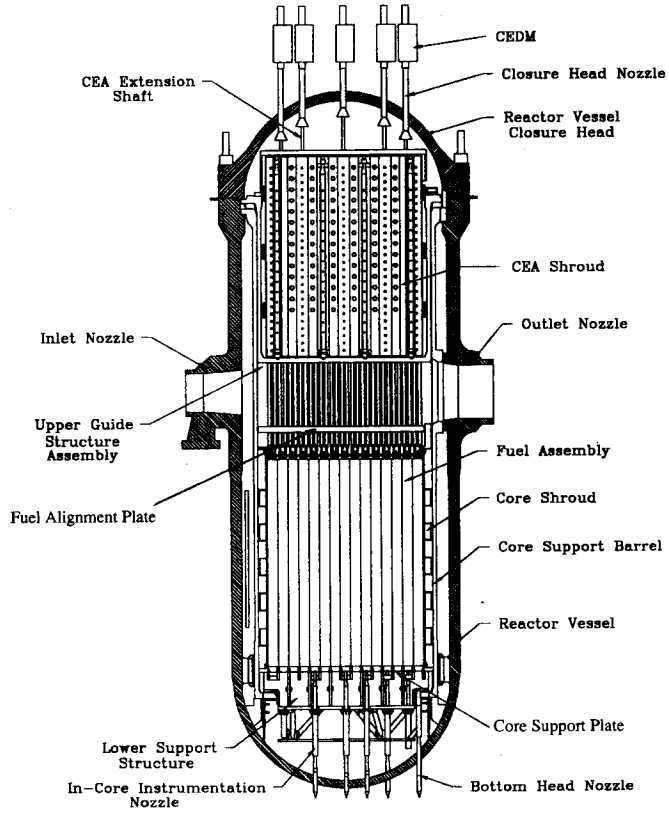

Fig. 1 Arrangement of reactor internals.

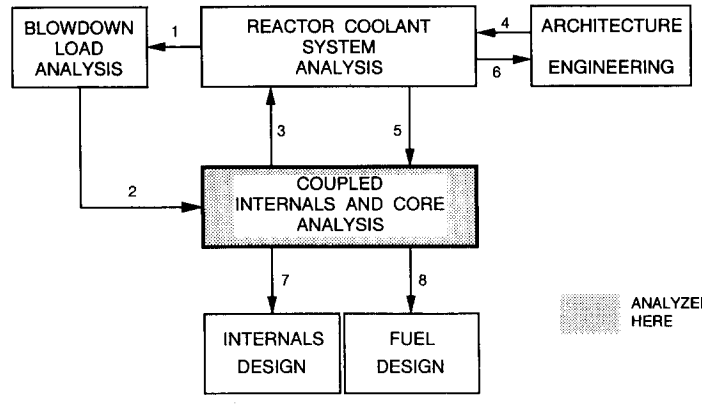

1. Break Location, Type, Area and Opening Time
2. Blow-down Load (Pressure, Flowrate) Time Histories
3. Internal Components Load (Force) Time Histories
4. Jet Impingement Loads and Sub-compartment Pressure Time Histories
5. Reactor Vessel Motions
6. Architecture Engineering Interface Data
7. Design Loads for Internal Components
8. Design Loads for Fuel Assembly

Fig. 2 Analysis procedure for pipe break excitation.

earthquake and secondary side pipe breaks.

For the purpose of assessing safety of the reactor core, various efforts for the dynamic response of the fuel assemblies in the horizontal direction have been made to understand dynamic characteristics (Jhung, *et al.* 1992a and 1992b, Jhung and Hwang 1994). By contrast with the horizontal direction, the axial responses are not investigated much because they are not relatively important from the structural integrity point of view (Jhung and Hwang 1993, Pace and DeMello 1988). But it should be pointed out that fuel assemblies should not lift off the core plates during the transient response.

In the present study, a method for dynamic analysis of the reactor internals and core is developed. The SHOCK computer code (Gabrielson 1966) which is used to solve the dynamic response of the lumped mass systems is updated to include a friction element. Two earthquakes-an operating basis earthquake (OBE) and a safe shutdown earthquake (SSE)-and six- 4 primary side and 2 secondary side-tributary pipe breaks are analyzed. Peak responses such as fuel assembly axial forces and lift-off characteristics are investigated.

2. Description of reactor internals and fuel assembly

The reactor internals are designed to support the reactor core, maintain the core in a coolable array, and guide the control element assemblies (CEAs) into the top of the core, and to constrain and protect the CEAs from coolant flow.

The components of the reactor internals are divided into two major parts consisting of the core support barrel (CSB) assembly and the upper guide structure (UGS) assembly. The flow skirt, although functioning as an integral part of the coolant flow path, is separate from the internals and is affixed to the bottom head of the reactor vessel. The arrangement of these components is shown in Fig. 1.

The core support barrel assembly includes the core support barrel, the lower support structure and incore instrumentation nozzle assembly, and the core shroud. The CSB is a right circular cylinder supported by a ring flange from a ledge on the reactor vessel. It carries the entire weight of the core. The lower support structure transmits the weight of the core to the core support barrel by means of a grid beam structure. The core shroud surrounds the core and minimizes the amount of bypass flow. The upper guide structure assembly includes the UGS barrel assembly, the CEA shroud assembly, the top hat, the holddown ring, and the heated junction thermocouple shroud assembly. The UGS assembly provides the CEAs a protection from coolant flow, and limits upward motion of the fuel assemblies.

The typical PWR core of 2825 MWt is composed of 177 fuel assemblies and 73 or more control element assemblies. The fuel assemblies are arranged to approximate a right circular cylinder with an equivalent diameter of 123 inches and an active length of 150 inches. The fuel assembly, which provides for 236 fuel rod positions (16×16 array), includes 5 guide tubes welded to 11 spacer grids and is closed at the top and bottom by end fittings. The guide tubes each displace four fuel rod positions and provide channels which guide the control element assemblies over their entire length of travel. In-core instrumentation is installed in the central guide tube of selected fuel assemblies. The incore instrumentation is routed into the bottom of the fuel assemblies through the bottom head of the reactor vessel. The outer guide tubes, spacer grids and end fittings form the structural frame of the assembly.

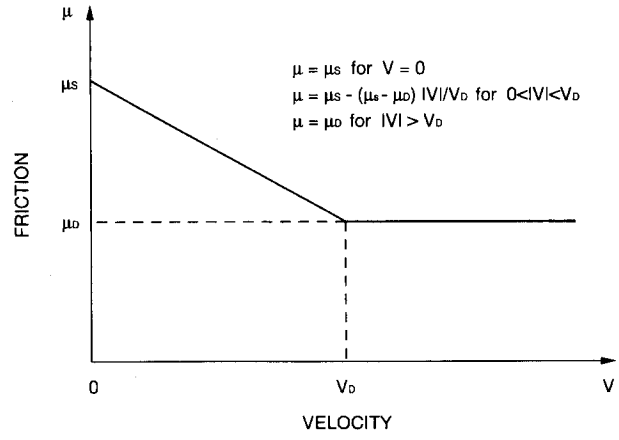

Fig. 3 Velocity dependent friction coefficient.

The fuel spacer grids maintain the fuel rod array by providing positive lateral restraint to the fuel rod but only frictional restraint to axial fuel rod motion. The grids are fabricated from preformed Zircaloy or Inconel strips (the bottom spacer grid material is Inconel) interlocked in an egg crate fashion and welded together. Each cell of the spacer grid contains two leaf springs and four arches. The leaf springs press the rod against the arches to restrict relative motion between the grids and the fuel rods.

3. Friction element theory

The slip-stick type of friction element is velocity dependent as shown in Fig. 3, where μ_S, μ_D and v_D are the static coefficient of friction, dynamic coefficient of friction and relative velocity at which μ_D is reached, respectively.

3.1. Friction force

Force which must be overcome by friction is calculated on the followings. Consider the system with two masses 1 and 2 to be sticking as shown in Fig. 4. If masses 1 and 2 are stuck

$$\ddot{x}_1' = \ddot{x}_2', \quad \dot{x}_1' = \dot{x}_2' \tag{1}$$

where prime (′) indicates terms after sticking occurs, and $\ddot{x}_i'$ and $\dot{x}_i'$ are stuck acceleration and stuck velocity, respectively. The velocity $\dot{x}_{eq}'$ of masses 1 and 2 after friction force is applied is calculated as:

$$\dot{x}_1 M_1 + \dot{x}_2 M_2 = \dot{x}_1' M_1 + \dot{x}_2' M_2 = \dot{x}_{eq}'(M_1 + M_2) \tag{2}$$

$$\therefore \quad \dot{x}_{eq}' = \frac{\dot{x}_1 M_1 + \dot{x}_2 M_2}{M_1 + M_2} \tag{3}$$

Applying the relation between impulse and momentum to mass I

$$\dot{x}_1 M_1 - F_f \Delta t = \dot{x}_{eq}' M_1 \tag{4}$$

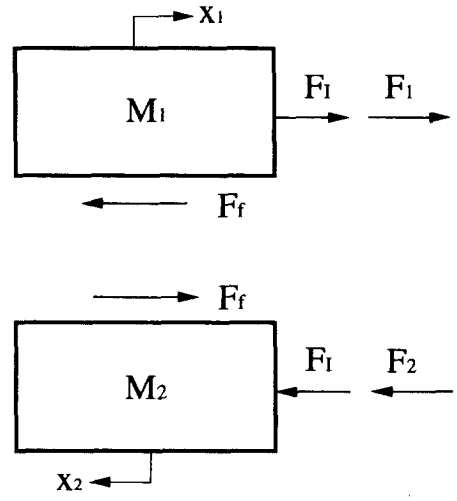

Fig. 4 Slip-stick type frictional masses.

where F_I is the force required to match the velocities. Substituting Eq. (3) into Eq. (4) gives

$$F_I=\frac{M_1M_2}{M_1+M_2}(\dot{x}_1-\dot{x}_2)/\Delta t \tag{5}$$

From the Newton's law for masses 1 and 2

$$\ddot{x}_1'M_1=F_1+F_I-F_f \tag{6}$$

$$\ddot{x}_2'M_2=-F_2-F_I+F_f \tag{7}$$

where F_f is the friction force. From Eq. (1)

$$\frac{F_1+F_I-E_f}{M_1}=\frac{-F_2-F_I+F_f}{M_2} \tag{8}$$

$$F_f=\frac{F_1M_2+F_2M_1+F_I(M_1+M_2)}{M_1+M_2}$$

$$=\frac{\ddot{x}_1M_1M_2-\ddot{x}_2M_2M_1+F_I(M_1+M_2)}{M_1+M_2}$$

$$\therefore\quad F_f=(\ddot{x}_1-\ddot{x}_2)\frac{M_1M_2}{M_1+M_2}+F_I \tag{9}$$

Substituting Eq. (5) into Eq. (9), the friction force is calculated as

$$F_f=\frac{M_1M_2}{M_1+M_2}\left[(\ddot{x}_1-\ddot{x}_2)+\frac{\dot{x}_1-\dot{x}_2}{\Delta t}\right] \tag{10}$$

If F_f is greater than normal force multiplied by friction coefficient (μN) the masses are slipping.

3.2. Acceleration

The accelerations after friction force is applied are calculated as follows:

(1) If masses are stuck

$$\dot{x}_1'=\dot{x}_2'=\frac{M_1\dot{x}_1+M_2\dot{x}_2}{M_1+M_2} \tag{11}$$

$$\ddot{x}_1'=\ddot{x}_2'=\frac{M_1\ddot{x}_1+M_2\ddot{x}_2}{M_1+M_2} \tag{12}$$

(2) If masses are slipping

1) $\dot{x}_1'>\dot{x}_2'$

$$\ddot{x}_1'=\frac{M_1\ddot{x}_1-F_{fD}}{M_1}=\ddot{x}_1-\frac{F_{fD}}{M_1}, \qquad \ddot{x}_2'=\ddot{x}_2+\frac{F_{fD}}{M_2} \tag{13}$$

2) $\dot{x}_1'<\dot{x}_2'$

$$\ddot{x}_1'=\ddot{x}_1+\frac{F_{fD}}{M_1}, \qquad \ddot{x}_2'=\ddot{x}_2-\frac{F_{fD}}{M_2} \tag{14}$$

3) $\dot{x}_1'=\dot{x}_2'$

$$\ddot{x}_1'=\ddot{x}_1, \qquad \ddot{x}_2'=\ddot{x}_2 \tag{15}$$

where $F_{fD}=\left[(\mu_S-\frac{(\mu_S-\mu_D)|\dot{x}_1'-\dot{x}_2'|}{v_D}\right]N$ for $0<|\dot{x}_1'-\dot{x}_2'|<v_D$,

$F_{fD}=\mu_D N$ for $|\dot{x}_1'-\dot{x}_2'|>v_D$.

The friction coefficients used here are $\mu_S=0.8$ and $\mu_D=0.2$, which were determined in experiments (Jhung, *et al.* 1992b). Summarizing these results, the calculational sequence of the friction force for each time step is shown in the flowchart of Fig. 5, where J is the step of the Runge-Kutta integration routine (Kuo 1972).

4. Analysis

4.1. Model development

The mathematical model of the internals and core consists of lumped masses and elastic beam elements to represent the beam-like behavior of the internals, and nonlinear elements to simulate the effects of gaps between components. Typical component gaps represented by nonlinear elements are the control element assembly guide tube and upper end fitting of the fuel assembly. At appropriate locations within the internals and core, nodes are chosen to lump the weights of the structure. The criterion for choosing the number and location of mass points is to provide for accurate representation of the dynamically significant modes of vibration for each of the internal components. For the beam element connecting two nodes, stiffness is calcula-

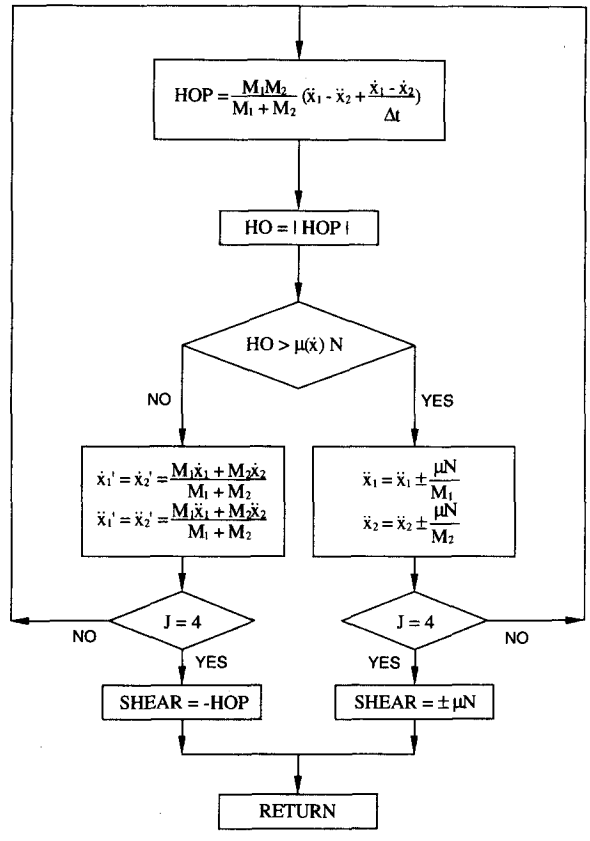

Fig. 5 Flowchart for calculation of friction force.

ted using the well known formula as

$$K_S = \frac{A_C E}{l} \tag{16}$$

where K_S=axial stiffness (lb/in),
A_C=cross-sectional area (in^2),
E=Young's modulus (psi),
l=length of segment (in).

If a beam has one or more changes in sections, the equivalent stiffness is the series sum of the parts. Stiffnesses for the complex structures such as flanges and tube bank assembly are determined by finite element analyses.

The core is modelled by grouping all fuel assemblies into a single grouping which includes the weight of the entire core. The vertical stiffness properties of the grouping are obtained by combining the individual stiffnesses of all the fuel assemblies in the core as springs in parallel. The fuel assembly grouping is subdivided into fuel rods and guide tubes with slip stick friction elements representing the connectivity between the two single stick models. This connectivity represents the friction force between the fuel rods and spacer grid arches and tabs. Both static and dynamic friction values are used. The fuel rods do not slip until the value of static friction is exceeded. When slipping of the fuel rods occurs, the resisting force is equal to the dynamic

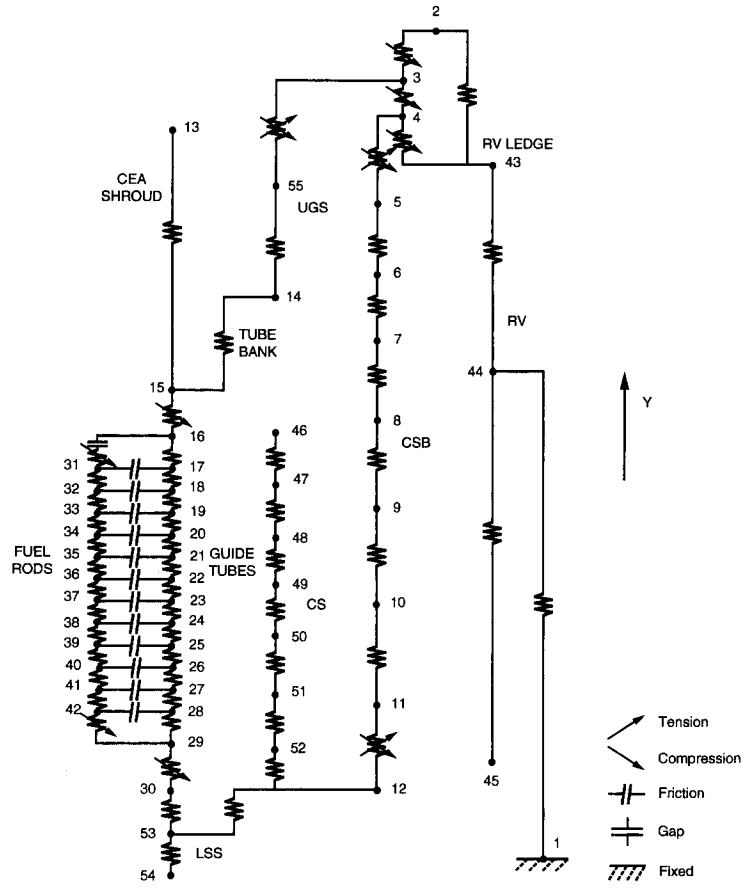

Fig. 6 Lumped mass model of reactor internals and core.

friction force. Beginning-of-life friction values are determined from tests by measuring the forces required to withdraw fuel rods from the bundle in an unirradiated condition. To determine end-of-life friction values, beginning-of-life experimental friction values are adjusted by factors based on the estimated relaxation of the grid material.

A typical coupled internals and core model in the vertical direction is shown in Fig. 6. The actual arrangement and detail in the model may vary with the function of plant design, and the magnitude and nature of the excitation.

4.2. Input excitations

The input excitations to the model consist of the hydraulic loads of internals and reactor vessel motions. The reactor vessel motions are determined from the reactor coolant system analysis and are acceleration time histories at the RV ledge. The internals hydraulic loads are calculated using a control volume formulation, where the internal structures and contained water are sectioned into solid plus fluid control volumes. Across each volume, the fluid momentum equation is solved as a function of time to compute the hydraulic loads. This method accounts for fluid pressure and momentum effects which act on all of the structures within each control volume.

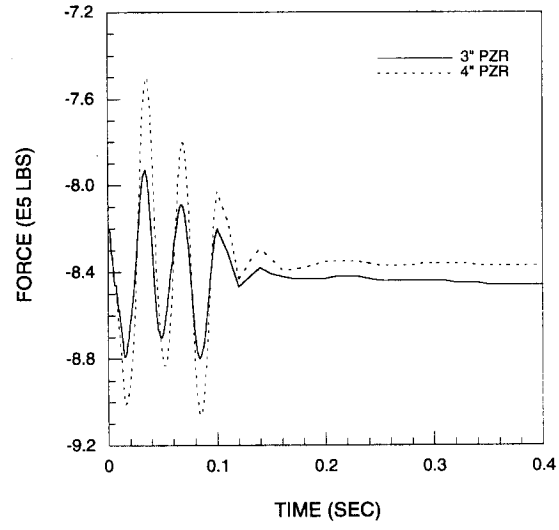

Fig. 7 Force time histories for PZR spray line break.

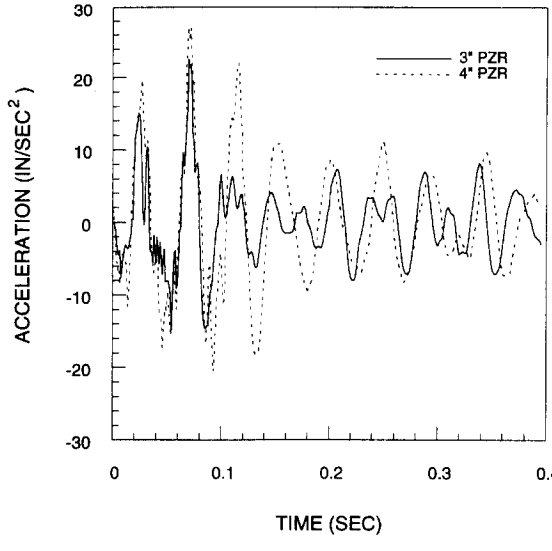

Fig. 8 RV motions for PZR spray line break.

The vertical loads of the core model are calculated using the pressure differentials across the ends plus the drag and fluid momentum terms. Separate loads are calculated for individual nodes presenting the fuel rods, guide tubes, upper-end-fitting (UEF) and lower-end-fitting (LEF).

Drag loads represented by fluid shear term are composed of two components-friction drag and form drag. These loadings are dependent on the channel equivalent diameter, channel cross-sectional area, fluid flow rate and fluid density. Frictional drag is apportioned to the guide tubes and to the fuel rods on the basis of fraction of total wetted perimeter adjacent to a given flow channel or subchannel. The only form losses present are due to the spacer grids. Crud effects are accounted for by multiplying the drag loads by an empirically determined factor. Time history plots of the total vertical hydraulic loads are shown in Fig. 7. Also, acceleration

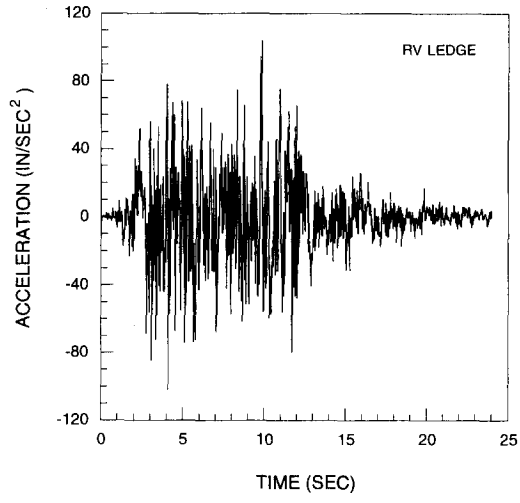

Fig. 9 RV motion for safe shutdown earthquake.

time histories of the RV ledge are shown in Fig. 8. For the earthquake excitations, no hydraulic loads exist, therefore the only forcing terms are the RV motions as shown in Fig. 9 for a safe shutdown earthquake.

4.3. Dynamic responses

Equilibrium conditions, prior to the application of the dynamic transient conditions, are established by determining the static displacements associated with the weight of the internals and core in water, preloads and the core drag steady state forces. These calculated static displacements are used as the initial conditions. Without these, some of the masses would be subjected to large accelerations because of the resulting force unbalance.

The responses of the fuel assemblies to the excitations were obtained using the SHOCK code, which integrates the equations of motion by the Runge-Kutta-Gill method for first-order differential equations and provides the time-history response of each component (Gabrielson 1966).

The integration time step was determined based on the impact pulse which is typically estimated to be (1/20)×(minimum period) (ASCE 1986).

5. Results and discussion

The result of the internals and core analysis consists of initial, total maximum and minimum loads on the reactor internals and core. The design loads are determined by subtracting initial loads from total loads and are used to assure the structural integrity of the components (Table 1). In addition, maximum axial direction fuel assembly end fitting displacements relative to the core support plate and fuel alignment plate are examined to insure that vertical height of the guide pins is not exceeded. Figs. 10 and 11 show a relative displacement time histories of the fuel assembly lower end fitting with respect to the core support plate for pressurizer (PZR) breaks and SSE, respectively. The non-zero values in the displacement time history are

Table 1 Axial forces of fuel assembly (unit=lbs)

Excitation	Fuel rods	Guide tubes
3″ PZR spray line nozzle break	225	20
4″ PZR spray line intermediate break	394	35
6″ PZR safety valve inlet nozzle break	73	6
3″ SDC long-term SI line intermediate break	198	18
SG feedwater economizer nozzle break	84	7
SG steam line nozzle break	106	9
Operating basis earthquake	279	25
Safe shutdown earthquake	506	45

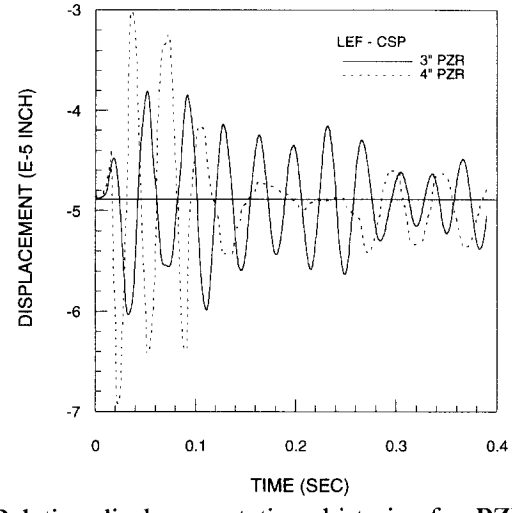

Fig. 10 Relative displacement time histories for PZR break.

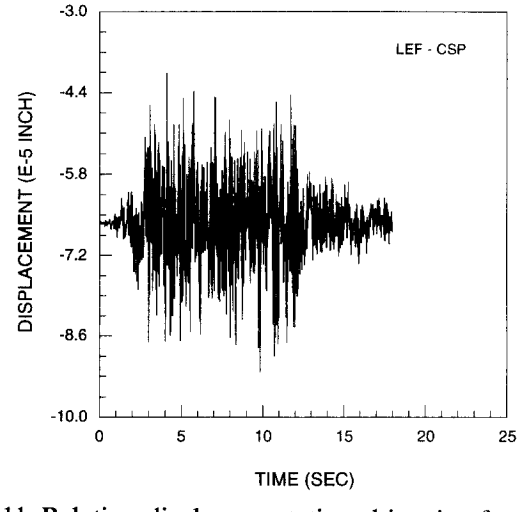

Fig. 11 Relative displacement time histories for SSE.

Table 2 Relative deflections of fuel assembly end fittings to core plates (unit=inch)

Excitation	LEF-CSP	UEF-FAP
3″ PZR spray line nozzle break	−.6035E-4	−.2057E0
4″ PZR spray line intermediate break	−.6927E-4	−.2066E0
6″ PZR safety valve inlet nozzle break	−.5229E-4	−.2047E0
3″ SDC long-term SI line intermediate break	−.5681E-4	−.2047E0
SG feedwater economizer nozzle break	−.7060E-4	−.1369E0
SG steam line nozzle break	−.7179E-4	−.1372E0
Operating basis earthquake	−.5191E-4	−.1339E0
Safe shutdown earthquake	−.4059E-4	−.1321E0

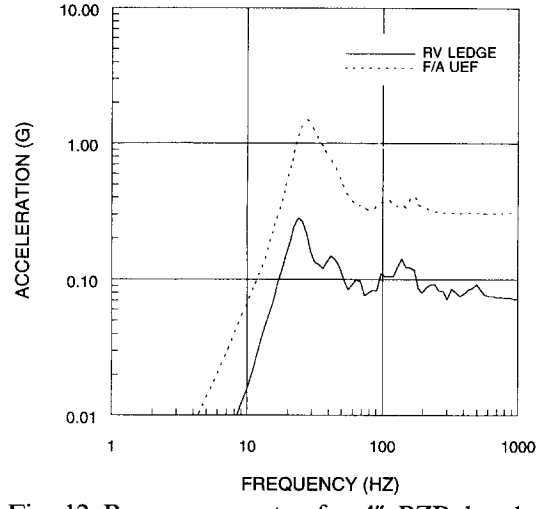

Fig. 12 Response spectra for 4″ PZR break.

associated with lifting fuel assemblies from the core plates. The amount of lift-off depends on the magnitude of the particular site specific excitation. The magnitude of this relative displacement is examined to ensure that vertical height of the guide pins is not exceeded. Guide pins have a height (3.125 inch) which is significantly larger than the relative displacement as indicated in Table 2.

The response spectra plot for RV ledge and UEF of fuel assembly are shown in Figs. 12 and 13 for PZR break and SSE, respectively. The peak of the fuel assembly spectra is amplified by a factor of 5.3 and 2.0 from the excitation point in the 4″ PZR break and earthquake, respectively. This indicates that the hydraulic loads considered in the pipe break analysis play an important part in the dynamic response. That's why the primary side pipe break produce higher responses than the secondary side pipe break, which results from the fact that the former uses RV motion and internals hydraulic loads as forcing functions but RV motion only is applied for the forcing term in the latter. The opposite was true for the horizontal response of the reactor core (Jhung, *et al.* 1992b).

The vertical analyses of various breaks indicated that the response obtained from a PZR spray line intermediate break would result in a maximum impact force, in this case an impact

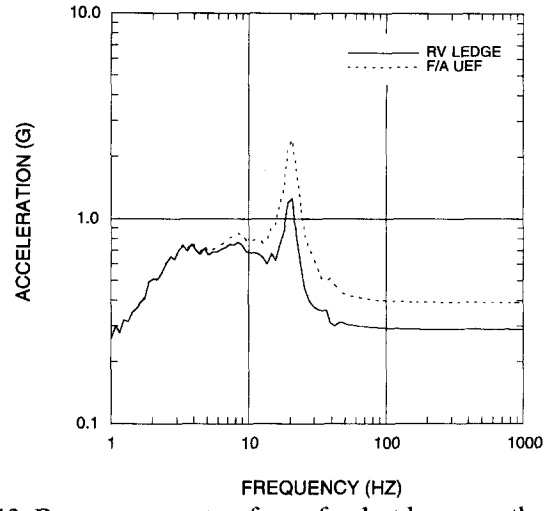

Fig. 13 Response spectra for safe shutdown earthquake.

load, of 394 lbs at the bottom of the fuel assembly. Using the maximum responses obtained from the faulted conditions, detailed stress analysis of the fuel assembly should show that it is structurally capable of resisting the hypothetical accident and also adequately designed to remain functional, i.e., the core coolable geometry will be maintained throughout the transient.

6. Conclusions

A method to calculate axial response of the reactor internals and core due to the dynamic excitations is developed to include the friction element for the interaction between fuel and grid cage. Dynamic analyses were performed for the two earthquake and six tributary pipe break excitations. The axial forces are calculated and the fuel assembly lift-off is examined to guarantee the proper operation of the nuclear power plant. As indicated in the results, the lift-off of fuel assembly does not exceed the guide pins even for the SSE condition. Also, it is shown that the responses due to the tributary pipe break conditions are lower than those of SSE in the faulted condition design.

References

ASCE, (1986), *Standard for Seismic Analysis of Safety-Related Nuclear Structures,* American Society of Civil Engineers, New York.

Daugherty, R.L. and Franzini, J.B. (1965), *Fluid Mechanics with Engineering Applications,* 6th ed., MacGraw Hill, New York.

Gabrielson, V.K. (1966), "SHOCK-A computer code for solving lumped-mass dynamic systems", Technical Report SCL-DR-65-34, Sandia Laboratories, Livermore, CA.

Hansen, A.G. (1967), *Fluid Mechanics,* John Wiley and Sons, New York.

Hildebrand, F.B. (1976), *Advanced Calculus for Applications,* 2nd ed., Prentice-Hall, Englewood Cliffs.

Jhung, M.J., Song, H.G. and Park, K.B. (1992a), "Dynamic characteristics of spacer grid impact loads

for SSE", *Journal of the Korean Nuclear Society,* **24**(2), 111-120.
Jhung, M.J., Park, K.B. and Sohn, G.H. (1992b), "Dynamic analysis of the reactor core for pipe break and seismic excitations", *Proceedings of the 7th International Conference on Pressure Vessel Technology,* Düsseldorf, Germany, June.
Jhung, M.J. and Hwang, W.G. (1993), "Seismic design criteria for the reactor vessel internals of the Korean Standard Nuclear Power Plant", *Proceedings of the Seminar on Pressure Vessel and Piping Technology,* Singapore, May.
Jhung, M.J. and Hwang, W.G. (1994), "Seismic behavior of a fuel assembly in the reactor core," *Seismic Engineering, ASME* PVP 275-1, New York.
Kuo, S.S. (1972), *Computer Applications of Numerical Methods,* Addison-Wesley, New York.
Pace, R.M. and DeMello, D.M. (1988), "Comparison of seismic analysis methodologies," *Seismic Engineering, ASME* PVP 144, New York.

Nomenclatures

A fluid flow area
A_C cross-sectional area
E Young's modulus
f Darcy friction factor
F force on the control volume transmitted through S
F_I force required to match velocity
F_f friction force
F_i force applied to mass i
g_c conversion factor of gravity for different unit
k loss factor
K_S axial stiffness
l length of segment
L control volume length
M_i mass i
N normal forcep fluid pressure
p fluid pressure
p_w fluid wetted perimeter
S_i control surfacev fluid velocity
v fluid velocity
v_D relative velocity at which μ_D is reached
V control volume
w fluid mass flow rate
x_i displacement of mass i
$\dot{x}_i$ velocity of mass i before friction force is applied
$\ddot{x}_i$ acceleration of mass i before friction force is applied
$\dot{x}_i'$ stuck velocity of mass i
$\ddot{x}_i'$ stuck acceleration of mass i
$\dot{x}_{eq}'$ velocity of masses 1 and 2 after friction force is applied
ρ fluid density
μ_D dynamic coefficient of friction
μ_S static coefficient of friction
τ non-hydrostatic portion of the stress tensor acting on the fluid

Appendix-Calculation of hydraulic force

Consider a general solid plus fluid control volume as shown in Fig. A1. The control surface is divided into 2 portions, S_1 and S_2, where S_2 is the portion of control surface cut by solid and $S_1=S-S_2$. The

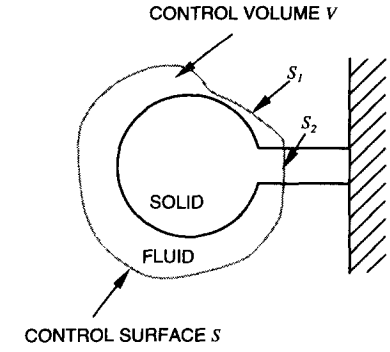

Fig. A1 General control volume representation.

fluid momentum equation from Hansen (1967) is

$$\frac{\partial}{\partial t}(\rho v)+\nabla\cdot\rho vv=-\nabla p+\nabla\cdot\tau+\rho\frac{g}{g_c} \tag{A1}$$

where ρ = fluid density,
v = fluid velocity,
p = fluid pressure,
τ = non-hydrostatic portion of the stress tensor acting on the fluid,
g_c = conversion factor of gravity for different unit.

Integrating equation (A1) over V and noting that no fluid is present in the solid region gives

$$\int_V \frac{\partial}{\partial t}(\rho v)\,dV+\int_V \nabla\cdot\rho vv\,dV=-\int_V \nabla p\,dV+\int_V \nabla\cdot\tau dV+\int_V \rho\frac{g}{g_c}\,dV \tag{A2}$$

Applying the divergence theorem (Hildebrand 1976) to the second term on the left and the first and second terms on the right, and expressing the forces transmitted to the control volume through S_1 and S_2 produces

$$\frac{\partial}{\partial t}\int_V(\rho v)\,dV+\int_{S_1}\rho vv\cdot d\boldsymbol{S}_1=-\int_{S_1}p d\boldsymbol{S}_1+\int_{S_1}\tau_{s_1}\cdot d\boldsymbol{S}_1+\int_V\rho\frac{g}{g_c}\,dV+\boldsymbol{F}_{SOLID} \tag{A3}$$

where $\boldsymbol{F}_{SOLID}$ is that portion of the force on the control volume transmitted through S_2, which may be thought of as the external force required to balance the hydraulic forces if the control volume is to be kept in equilibrium. Then $\boldsymbol{F}=-\boldsymbol{F}_{SOLID}$ is the hydraulic force that acts on the control volume and equation (A3) may be written as

$$\begin{aligned}\boldsymbol{F}&=-\int_{S_1}p d\boldsymbol{S}_1\int_V\rho\frac{g}{g_c}\,dV-\int_{S_1}\rho vv\cdot d\boldsymbol{S}_1-\frac{\partial}{\partial t}\int_V(\rho v)\,dV+\int_{S_1}\tau_{s_1}\cdot d\boldsymbol{S}_1\\&=\boldsymbol{F}_1+\boldsymbol{F}_2+\boldsymbol{F}_3+\boldsymbol{F}_4+\boldsymbol{F}_5\end{aligned} \tag{A4}$$

In this manner, it is seen that the hydraulic force is made up of 5 components as

$\boldsymbol{F}_1$ = force due to fluid pressure,
$\boldsymbol{F}_2$ = force due to fluid weight,
$\boldsymbol{F}_3$ = force due to momentum change within the control volume,
$\boldsymbol{F}_4$ = force due to momentum storage within the control volume,
$\boldsymbol{F}_5$ = force due to shear.

Now it is necessary to specialize the treatment to the two types of flow situation-a channel passing through a control volume and a channel passing adjacent to a control volume as shown in Fig. A2 (a) and (b), respectively, where the positive flow direction is up, gravity acts down, control volume length

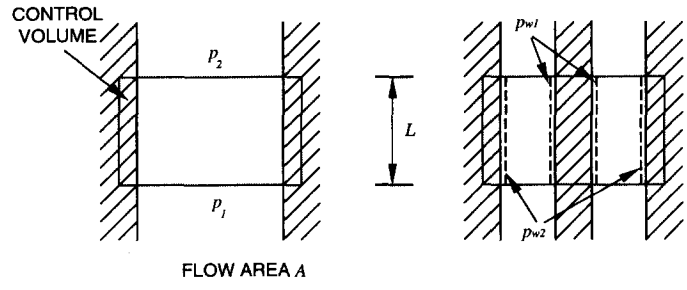

Fig. A2 Two types of flow situations.

is L, pressure at the upper control surface is p_2 and pressure at the lower control surface is p_1.

For the case of the channel passing through a control volume, F_5 vanishes and F_1 through F_4 in the flow direction become

$$F_1=-[p_2A-p_1A]=p_1A-p_2A,$$

$$F_2=-\rho AL\frac{g}{g_c},$$

$$F_3=-[\rho Av_2^2-\rho Av_1^2]=-w_2v_2+w_1v_1=\frac{w_1^2}{\rho A}-\frac{w_2^2}{\rho A}=0,$$

$$F_4=-\frac{\partial}{\partial t}[\rho vAL]=-L\frac{dw}{dt}.$$

Therefore

$$F=p_1A-p_2A-\rho AL\frac{g}{g_c}-L\frac{dw}{dt} \tag{A5}$$

Note that the force due to momentum change is zero because fluid mass flow rate w and flow area A are uniform at the upper and lower control surfaces.

For the case of the channel passing adjacent to a control volume, only F_5 in equation (A4) is nonzero, which is usually expressed as the sum of a friction drag and a form drag in the vertical direction. Friction drag is expressed in terms of a Darcy friction factor f (Daugherty and Franzini, 1965) as

$$\tau_{FRICTION}=\frac{1}{8g_c}f\rho v|v| \tag{A6}$$

where writing $v|v|$ accounts for sign. Then the total frictional shear force exerted by the fluid is

$$F_{FRICTION}=\tau_{FRICTION}p_wL \tag{A7}$$

where wetted perimeter $p_w=p_{w1}+p_{w2}$. This force is apportioned to the various structures according to fraction of total wetted perimeter adjacent to each substructure. The fraction ϕ of the total channel wetted perimeter adjacent to the control volume is

$$\phi=\frac{p_{w1}}{p_{w1}+p_{w2}} \tag{A8}$$

then

$$F_{FRICTION,C.V.}=\tau_{FRICTION}p_wL\phi=\frac{1}{8g_c}f\rho v|v|p_wL\phi$$

$$=f\frac{1}{8g_c\rho A^2}w|w|p_wL\phi \tag{A9}$$

Form drag is expressed in terms of a loss factor k that must be determined empirically (Daugherty and Franzini, 1965) as

$$F_{FORM,C.V.}=k\frac{1}{2g_c\rho A}w|w| \tag{A10}$$

Therefore the total force acting on the control volume due to adjacent channel is

$$F=f\frac{1}{8g_c\rho A^2}w|w|p_wL\phi+k\frac{1}{2g_c\rho A}w|w| \tag{A11}$$